Temperature dependence of CH3I self-broadening coefficients in the ν6 fundamental

L. Troitsyna, A. Dudaryonok, J. Buldyreva, N. Filippov, N. Lavrentieva

Version of Record: https://www.sciencedirect.com/science/article/pii/S0022407319307812
Manuscript_a6e5dda66870a57fec62fe8b7742a2d3

Temperature dependence of CH_3I self-broadening coefficients in the ν_6 fundamental

L. Troitsyna[a,*], A. Dudaryonok[b], J. Buldyreva[a], N. Filippov[c], N. Lavrentieva[b]

[a] *Institut UTINAM UMR CNRS 6213, Université Bourgogne Franche-Comté, 16 route de Gray, 25030 Besançon cedex, France*
[b] *V.E. Zuev Institute of Atmospheric Optics, 1 Akademishian Zuev square, 634021 Tomsk, Russia*
[c] *St Petersburg State University, 7/9 Universitetskaya emb., 199034 St Petersburg, Russia*

Abstract

Temperature dependence of methyl iodide self-broadening coefficients in the fundamental ν_6 band is evaluated theoretically by the use of a semi-classical and a semi-empirical approaches in the range 200–400 K recommended for HITRAN. In the absence of not-room-temperature measurements, comparisons are performed solely between line-width sets computed by the two methods at some fixed temperatures. Traditional temperature exponents as well as parameters of the recently suggested double power law [*JQSRT 2018;217:440-52*] (going beyond the considered temperature range) are determined for (J,K)-lines with $0 \leq J \leq 70$, $K \leq 20$ requested by spectroscopic databases. Because of the negligible vibrational dependence, these data can be safely used for other perpendicular and parallel bands studied in atmospheric applications.

Keywords: Methyl iodide, Self-broadening coefficients, Temperature dependence, Temperature exponents, Double power law, Perpendicular bands, Semi-classical calculations, Semi-empirical calculations, Atmospheric applications

1. Introduction

The interest to spectroscopic parameters of methyl iodide lines has risen abruptly over the last few years due to its environmental significance (source of iodine atoms destroying the ozone layer) and the needs of nuclear safety and radio protection (part of the released radioactivity not trapped on filters). Indeed, CH_3I is one of so-called volatile organic halocarbons that, though short-lived, influence the ozone concentration in the upper troposphere and lower stratosphere [1]. Moreover, it is one of possible pollutants in case of a nuclear accident [2] and is of great danger for human's health as iodine-131 containing compound. Although the natural production of methyl iodide is limited to a few sources (marine algae and bacteria [3], terrestrial fungi and bacteria [4], rice plantations [5]) and its concentration

*Corresponding author larisa.troitsyna@univ-fcomte.fr

in the atmosphere reaches solely 1–3 pptv [6], it may be successfully detected owing to its numerous IR-active bands.

Despite the growing needs for atmospheric monitoring, line-shape parameters for this molecule are still absent from spectroscopic databases such as e.g. HITRAN [7] and GEISA [8]. This lack can be partly attributed to the existence of Coriolis interactions inside low-lying manifolds of vibrational levels (for instance, between v_6=1 and v_3=2 states) and to the presence of well-spaced nuclear quadrupole hyperfine structure observable even in the IR region and complicating the assignment of spectral lines. Separate studies of line positions and intensities in several IR-absorption bands had been reported during decades (see Ref. [9] for a short review) before the need of exhaustive line-parameters sets was generally admitted by the spectroscopic community. In order to generate line lists for CH_3I detection, a series of works on line positions and intensities has been performed very recently for the ν_6, $2\nu_3$ [9, 10] and ν_5, $\nu_3 + \nu_6$ [11] bands. Such essential molecular parameters as transition moments for the $2\nu_3$, ν_6 [10] and ν_5, $\nu_3 + \nu_6$ [11] interacting bands as well as high-precision rotational constants for the ground, $v_2 = 1$, $v_3 = 2$ and $v_6 = 1$ states [9] were determined. As for the pressure-broadening and -shifting coefficients, their measurements have been initiated only in the year 2000 by the work of Belli et al. [12], who focused on the hyperfine components of the transition ($J = 10 \rightarrow 9, Kl = 9$) of the ν_6 band, and pushed further by Hoffman and Davies [13], who published self-, O_2- and N_2-broadening coefficients for some lines in the ν_5 fundamental. First line lists of the room-temperature ν_6 CH_3I lines self-broadened [14] and both self- and N_2-broadened [15] have been suggested solely in 2019. The work [14] besides experimental values provided theoretical calculations by a semi-classical (SC) [16] and a semi-empirical (SE) methods [17]. However, neither experimental results nor theoretical estimates have been reported up to now for the temperature dependence characteristics of methyl iodide line widths and shifts.

The present work aims to furnish this missing information for transitions in the ν_6 band which, being located in the 11 μm transparency window, is of particular interest for terrestrial atmosphere monitoring. Both theoretical methods employed previously [14] are used to evaluate line widths in the temperature range 200–400 K and extract their temperature-dependence characteristics. Pressure-induced shifting is not considered because of the absence of vibrationally dependent isotropic potential for the semi-classical calculations and unavailability of data on line shifts for determination of semi-empirical model parameters. Computations are done for all 6 sub-branches of the the ν_6 band ($^{R,P}P$, $^{R,P}Q$, $^{R,P}R$,) in large intervals of rotational quantum numbers ($0 \leq J \leq 70$, $K \leq 20$) requested by spectroscopic databases.

In the next section we remind briefly the salient features of the semi-classical and semi-empirical approaches. Section 3 is devoted to comparison of line widths computed by these two methods at various temperatures. Two different ways to model the temperature dependence (traditional temperature exponents and the recently suggested double power law [18]) are considered in detail in Sec. 4. The final section summarizes the main conclusions of our work. Numerical values for the obtained temperature-dependence parameters are provided in Supplementary material.

2. Semi-classical and semi-empirical approaches

2.1. Semi-classical method

For the transition $i(J_i, K_i) \rightarrow f(J_f, K_f)$ collisional line half-width is expressed by[1] [22]

$$\gamma_{if} = \frac{n\overline{v}}{2\pi c} \int_0^\infty 2\pi b db \langle 1 - e^{-ReS_2} \rangle_{J_2} \tag{1}$$

with the number density of perturbing particles n, mean thermal velocity $\overline{v}$, impact parameter b, average on the rotational states of perturber $\langle ... \rangle_{J_2}$ and the real part of the second-order contributions to the scattering matrix S_2 composed of $S_{2,i2}$, $S_{2,f2}$ and $S_{2,f2i2}$ terms. For the case of two symmetric tops these terms read [16]

$$\begin{aligned} S_{2,i2} &= -\frac{\hbar^{-2}}{2(2J_i+1)(2J_2+1)} \\ &\times \sum_{\substack{J_i' K_i' M_i' \\ J_2' K_2' M_2' M_i M_2}} \left| \int_{-\infty}^{\infty} dt e^{i\omega_{J_i K_i J_2 K_2, J_i' K_i' J_2' K_2' } t} \langle J_i K_i M_i J_2 K_2 M_2 | V_{aniso}(\vec{r}(t)) | J_i' K_i' M_i' J_2' K_2' M_2' \rangle \right|^2, \end{aligned} \tag{2}$$

$$\begin{aligned} S_{2,f2i2} &= -\frac{\hbar^{-2}}{(2J_i+1)(2J_2+1)} \sum_{J_2' K_2'} \sum_{\substack{M_i M_i' M_f M_f' \\ M_2 M_2' M}} C^{J_i M_i}_{J_f M_f \rho\sigma} C^{J_i M_i'}_{J_f M_f' \rho\sigma} \\ &\times \int_{-\infty}^{\infty} dt e^{i\omega_{J_2' K_2' J_2 K_2} t} \langle J_f K_f M_f' J_2' K_2' M_2' | V_{aniso}(\vec{r}(t)) | J_f K_f M_f J_2 K_2 M_2 \rangle \\ &\times \int_{-\infty}^{\infty} dt' e^{i\omega_{J_2 K_2 J_2' K_2'} t'} \langle J_i K_i M_i J_2 K_2 M_2 | V_{aniso}(\vec{r}(t')) | J_i K_i M_i' J_2' K_2' M_2' \rangle \end{aligned} \tag{3}$$

(the equation for $S_{2,f2}$ is obtained by replacing index i by f in Eq. (2)). The frequencies $\omega_{J_i K_i J_2 K_2, J_i' K_i' J_2' K_2'}$ in Eq. (2) are the sums of two frequencies $\omega_{J_i K_i J_i' K_i'}$ and $\omega_{J_2 K_2 J_2' K_2'}$ corresponding to the collision-induced transitions in the active and perturbing molecules. The Clebsch-Gordan coefficients $C^{J_i M_i}_{J_f M_f \rho\sigma}$ in Eq. (3) describe the coupling between the active molecule and the external field ($\rho = 1$ for IR absorption). For practical integration with a trajectory model the impact parameter b is replaced by the distance of the closest approach r_c and the relative motion is governed by the isotropic potential traditionally taken in the

[1] We do not employ the modified formula [19] since for a similar CH_3Cl- CH_3Cl system it was found [20] to worsen the agreement with experiment. Moreover, the line coupling effects [21] are also ignored since for the strongly polar CH_3I molecule the expected overestimation of line broadening is rather due to the deep isotropic potential strongly perturbing the relative molecular motion.

Lennard-Jones 12-6 form. In the case of the exact trajectories Eqs. (2) and (3) reduce to [14]

$$S_{2,i2} = \frac{2r_c^2}{\hbar^2\overline{v}^2} \sum_{\substack{l_1 l_2 l \\ k_1 k_2}} \frac{1}{(2l_1+1)(2l_2+2)} \sum_{\substack{J_i' K_i' \\ J_2' K_2'}} \left(C^{J_i'-K_i'}_{J_i-K_i l_1 k_1}\right)^2 \left(C^{J_2'-K_2'}_{J_2-K_2 l_2 k_2}\right)^2 f^{k_1 k_2}_{l_1 l_2 l} \ , \tag{4}$$

$$S_{2,f2i2} = -\frac{2r_c^2}{\hbar^2\overline{v}^2} \sum_{\substack{l_1 l_2 l \\ k_1}} \frac{(-1)^{\rho+l_2+l}}{(2l_1+1)(2l_2+2)} D(J_i J_f K_i K_f; \rho l_1) \sum_{\substack{J_i' K_i' \\ J_2' K_2'}} \left(C^{J_2' K_2'}_{J_2 K_2 l_2 k_2}\right)^2 f^{0 k_2}_{l_1 l_2 l} \ . \tag{5}$$

The resonance functions $f^{k_1 k_2}_{l_1 l_2 l}$ can be found in [16] and the coefficients $D(J_i J_f K_i K_f; \rho l_1) = (-1)^{J_i+J_f}\sqrt{(2J_i+1)(2J_f+1)} C^{J_i K_i}_{J_i K_i l_1 0} C^{J_f K_f}_{J_f K_f l_1 0} W(J_i J_f J_i J_f; \rho l_1)$ including the Racah coefficients $W(J_i J_f J_i J_f; \rho l_1)$ depend on the considered sub-branch.

In the present work the Lennard-Jones parameters were taken as ε = 232.86 K and σ = 3.6367 Å [23]. The anisotropic potential was modeled by the leading electrostatic interactions (dipole-dipole, dipole-quadrupole and quadrupole-quadrupole) according to the common practice for the strongly interacting molecules of CH_3X type (e.g. CH_3F [24], CH_3Br [25], CH_3Cl [26], and CH_3CN [27]). The dipole moment value μ=1.1613 D and the quadrupole moment value Q=10.70 DÅ were those of Refs. [28] and [29], respectively. The molecular rotational constants A_0=5.17394986 cm^{-1}, B_0=0.25021630 cm^{-1} for the ground state and A_6=5.20864873 cm^{-1}, B_6=0.24942867 cm^{-1} for the v_6=1 state [9] were used. The rotational populations were accounted for up to J_{max} = 90 for active molecules and up to $J_{2\ max}$ = 106, $K_{2\ max}$ = 22 for perturbing molecules, the resonance perameter was up to $k_{c\ max}$ = 25, and the maximal r_c value was 35 Å, which ensured convergence of line widths within 1%. These maximal parameters values were considered as sufficient, given the high CPU cost of exact-trajectory computations.

2.2. Semi-empirical method

The key idea of the semi-empirical approach [17] is to simplify the Robert-Bonamy expression to an Anderson-Tsao-Curnutte form [30]

$$\gamma_{if} = B(i,f) + \sum_l D^2(ii'|l) P_l(\omega_{ii'}) + \sum_l D^2(ff'|l) P_l(\omega_{ff'}) + ... \tag{6}$$

The first term in the rhs of this equation represents the contribution from Anderson's cut-off procedure:

$$B(i,f) = \frac{n}{c} \sum_k \rho(k) b_0^2(k,i,f), \tag{7}$$

where ρ is the thermal population of the perturber's level with a set of quantum numbers k and b_0 is the cut-off radius. The terms $D^2(ii'|l)$ and $D^2(ff'|l)$ in Eq. (6) denote the transition strengths corresponding to the l-th rank multipoles and P_l are the so-called efficiency functions related to different scattering channels. These efficiency functions are further seen as products of the analytical Anderson's efficiency functions P_l^A and correction factors $C_l(\omega)$. The specific form of the correction factor is chosen in function of line-width

J-dependence at small K and its parameters are fitted on some experimental values. In such a way, corrections for the real trajectory curvature and vibrational effects as well as corrections to the scattering matrix are taken into account and ensure reliable recovering of experimental results.

For the aims of the present work, since the J-dependences of line widths at small K demonstrate regular behavior, the correction factor was taken in the traditional two-parameter form

$$C_l(\omega) = \frac{c_1}{c_2\sqrt{J_i}+1} \tag{8}$$

and the model parameters c_1 and c_2 were fitted on some experimental line widths in the $^{\mathrm{R}}$Q sub-branch.[2] In the anisotropic potential the leading electrostatic as well as induction and dispersion contributions were accounted for.

3. Results and discussion

3.1. Comparison of SC and SE results at various temperatures

Computations by both theoretical methods were performed for 5 temperatures in the temperature range 200–400 K: 200, 250, 296, 350 and 400 K. The results for a particular case of $^{\mathrm{R}}$R-transitions with K=0 are visualized in Fig. 1 (an example of numerical values is given in Table 1). Same scaling intervals are kept for the broadening axis in all panels, in order to better appreciate the influence of the temperature on the computed results. The left upper panel shows the overlaid plot of SC and SE values at five chosen temperatures. The general decrease of line widths with increasing temperature is well reproduced (life-time of each level grows because of larger Boltzmann distributions of rotational populations), and for high J values the calculations become nearly temperature-independent (a quickly rotating top is very stable and unperturbed by collisions with surrounding molecules). The left lower panel contains a detailed comparison for the room temperature. In addition to the SC-SE results, it comprises available measurements [14] and the SC values obtained with a r_c cut-off at 24 Å which provides the best match of experimental data. This cut-off is of interest since it was suggested in the literature [25] for the case of highly polar self-perturbed molecules of CH_3X type to avoid the problem of line-width overestimation by semi-classical approaches. For the room-temperature CH_3Cl line widths, for example, the cut-off at 22 Å resulted in very realistic K-dependences [20] and, providing line widths for high K values inaccessible experimentally for SE-parameters fitting, allowed reliable restoring of experimental values at 200 K [31]. For a lower (250 K) and a higher (350 K) temperatures (two rhs panels), the 35 Å-semi-classical and semi-empirical results are quite close. Since the SE values are expected to be quite realistic (the SE model parameters were shown to be temperature-independent), the 24 Å-cut-off in SC values seems to underestimate the broadening too much and, therefore, seems to be inappropriate for extracting the temperature-dependence parameters considered in the following subsections.

[2] Fits were also done for some experimental data sets in the $^{\mathrm{R}}$P and $^{\mathrm{R}}$R sub-brunches resulting in slight modifications of c_1, c_2 values (see [14] for more details).

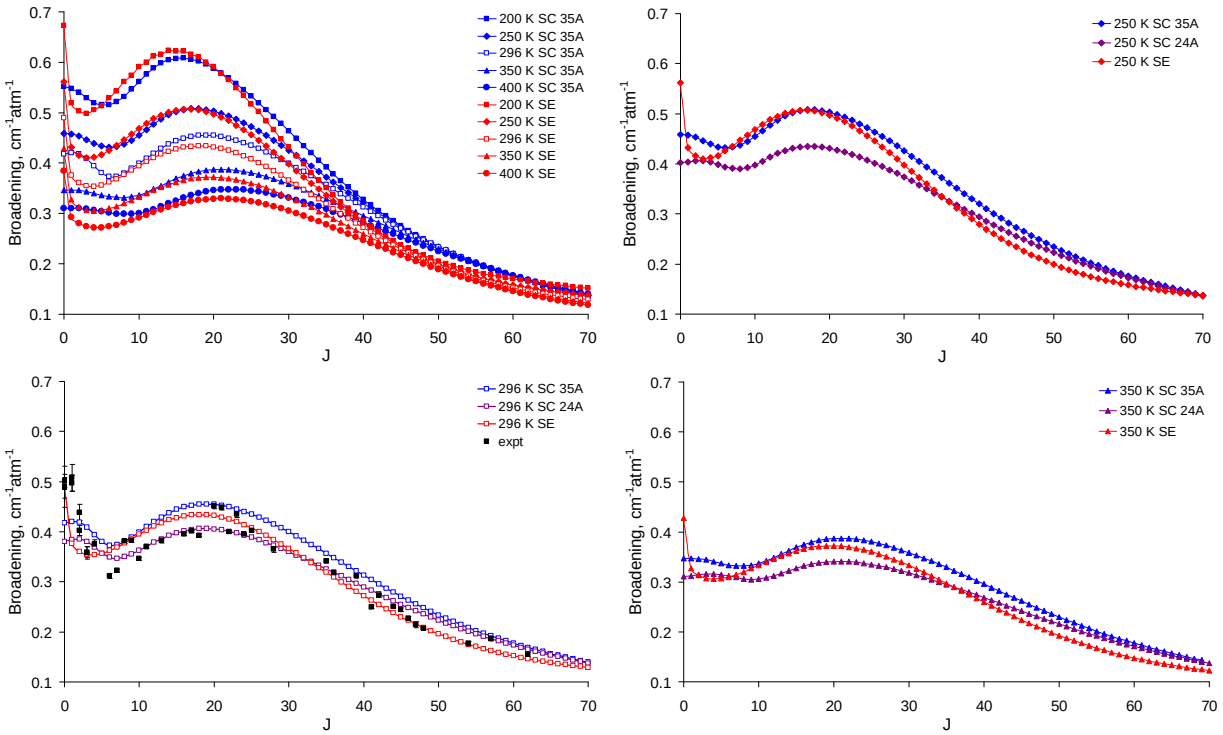

Figure 1: Comparison of CH_3I self-broadening coefficients computed at various temperatures by the semi-classical (SC) and semi-empirical (SE) approaches for the ^{R}R transitions with K=0 in the ν_6 band. Experimental values [14] are shown solely for 296 K since unavailable at other temperatures. The SC results with the cut-off of the intermolecular distance at 24 Å (giving the best agreement with the available measurements) are also plotted for completeness.

3.2. Determination of temperature exponents

To characterize the temperature dependence of CH_3I line broadening we consider first the traditional approach making use of the so-called temperature exponents N:

$$\gamma_{if}(T) = \gamma_{if}(T_{ref}) \left(\frac{T_{ref}}{T} \right)^N \tag{9}$$

with the reference temperature T_{ref} usually chosen as 296 K for atmospheric applications. It should be kept in mind that for many molecules this equation is applicable solely in narrow temperature intervals about 100 K.

The quality of linear log-log fits for the semi-classical results as well as the influence of the cut-off at 24 Å is illustrated in Fig. 2 for some K=0 transitions in the ^{R}R-sub-branch. Because of the well known drawback of the semi-classical approach to underestimate the broadening at few first J values, for the transition (0,0) the non-linearity is already visible

Table 1: Sample of SC- and SE-calculated line widths in ($cm^{-1}atm^{-1}$) for transitions in the ^{R}R sub-branch for $K = 0$. Semi-classical values correspond to computations with $r_c \leq 35$ Å.

	SC					SE				
J	200 K	250 K	296 K	350 K	400 K	200 K	250 K	296 K	350 K	400 K
0	0.5510	0.4583	0.4177	0.3467	0.3101	0.6724	0.5616	0.4903	0.4286	0.3851
1	0.5476	0.4570	0.4200	0.3467	0.3104	0.5196	0.4319	0.3757	0.3274	0.2934
2	0.5400	0.4532	0.4184	0.3461	0.3103	0.5038	0.4159	0.3605	0.3131	0.2800
3	0.5292	0.4467	0.4092	0.3439	0.3092	0.4984	0.4101	0.3545	0.3072	0.2742
4	0.5198	0.4394	0.3944	0.3404	0.3069	0.5057	0.4120	0.3541	0.3055	0.2720
5	0.5153	0.4342	0.3805	0.3366	0.3040	0.5134	0.4164	0.3566	0.3066	0.2722
6	0.5160	0.4321	0.3732	0.3337	0.3014	0.5298	0.4255	0.3622	0.3098	0.2741
7	0.5216	0.4332	0.3737	0.3320	0.2996	0.5425	0.4347	0.3689	0.3144	0.2774
8	0.5320	0.4374	0.3798	0.3319	0.2988	0.5616	0.4467	0.3772	0.3201	0.2815
9	0.5460	0.4450	0.3890	0.3334	0.2991	0.5740	0.4571	0.3856	0.3265	0.2865
10	0.5616	0.4551	0.3992	0.3367	0.3008	0.5911	0.4690	0.3945	0.3331	0.2916

and strongly pronounced for both converged ("SC 35 Å" curve) and truncated ("SC 24 Å" curve) line widths. For the transition (5,0) the behavior is nearly linear for both series of broadening coefficients, however the converged line widths result in a slightly better linear fit with a more abrupt slope (closer to the SE value 0.915 than the 24 Å-one). Similarly, for higher J the 35 Å-curves provide "more linear" dependencies and higher values of the temperature exponents. We can conclude from this figure that the SC approach, even limited to 3-temperature fits (250-350 K range), is characterized in general by nonlinear dependencies in the log-log scale and, therefore, is not very reliable for estimating the temperature exponents.

Fig. 3 presents a similar analysis of log-log dependencies for the semi-empirical approach. Instead of the full or truncated intermolecular distances related to the SC values and discussed above, the secondary aspect here is to probe the validity of the use of SE data computed for 200 K. Indeed, considering the isotropic interaction potential depth for CH_3I-CH_3I ($\varepsilon = 232.86\ K$ [23]), one could have a doubt on the reliability of semi-classical/semi-empirical [3] calculations for this temperature. On the other hand, the SE values do not demonstrate any irregularity in the calculated line widths when going down to 200 K, so that the question weather or not the 200 K results should be included is worth contemplating. As can be seen in Fig. 3, the dependencies are linear ($J \lesssim 20$) or nearly linear ($J \gtrsim 20$), and adding the 200 K-results does not influence strongly the extracted temperature exponents. It means that for most lines with low and middle values of the rotational quantum numbers the linear regression of SE results furnishes reliable values of the temperature exponents (confidence in the range 1-0.99). Solely the cases of high J (and high K) give relatively small line

[3] The semi-empirical approach is basically of a semi-classical nature.

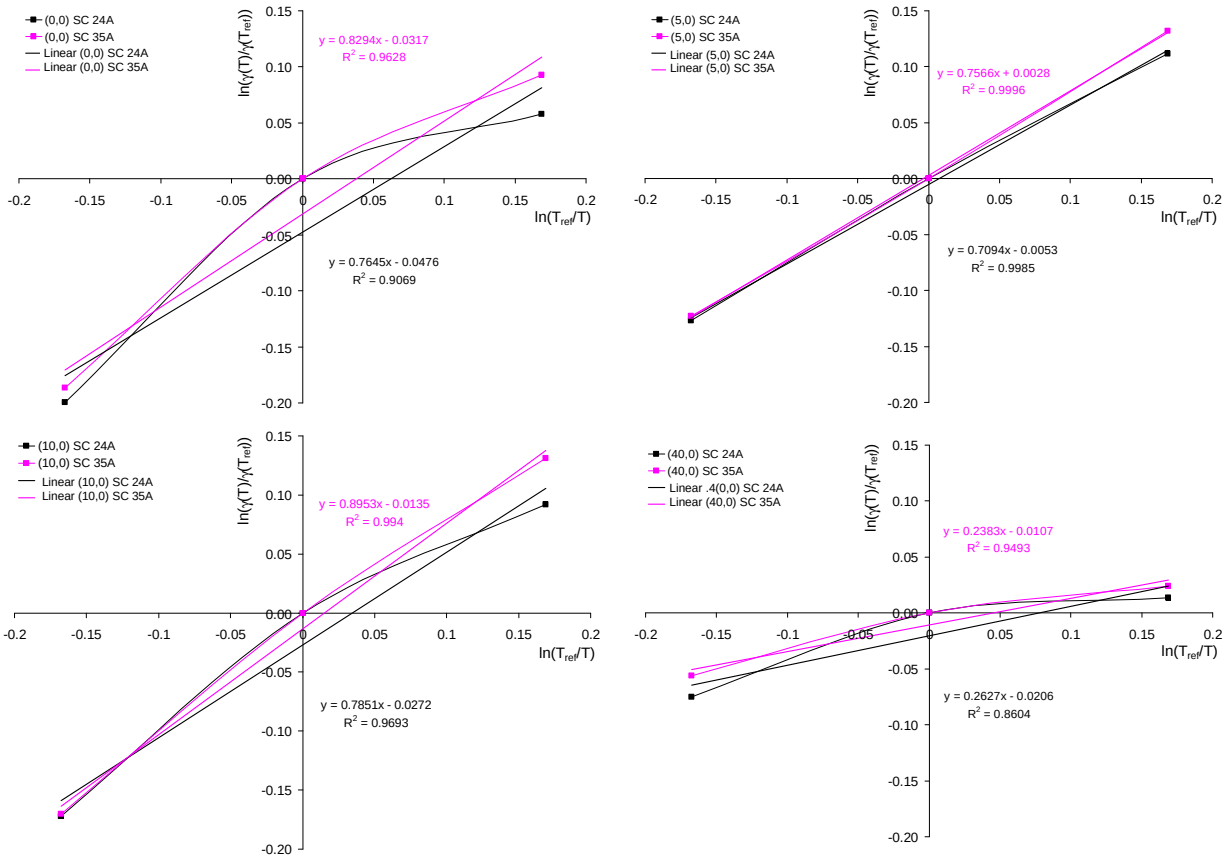

Figure 2: Linear fits of semi-classical results in log-log coordinates. Except a small region $J \approx 5$, the dependencies are visibly non linear. The use of the fully converged ($r_c \leq 35$ Å) linewidths improves slightly but not sufficiently the results obtained with the cut-off at 24 Å.

widths which leads to less trusty results (confidence of 0.97 or below). Therefore, in the case of temperature exponents the SE approach can be considered as more appropriate for extracting the temperature dependence characteristics than the SC method.

A more general view of the differences between the SE temperature exponents extracted without ("4T" curves) and with 200 K ("5T" curves) is presented in Fig. 4 for $^{\mathrm{R}}$R transitions corresponding to some given K values (K=0, 10 and 20). The first couple of curves for K=0 confirms the conclusions of Fig. 3 that for $J \lesssim 20$, because of the linear log-log dependence, no substantial differences are observed between the temperature exponents deduced with 4 and 5 temperatures; a similar absence of differences is in the vicinity of $J \approx 49$ where the slope changes the sign. In the other J-intervals for $K = 0$ and for the other-K pairs of curves the differences are about 0.04 which falls however in the error-bar range, so that the J-dependencies of temperature exponents corresponding to 4 and 5 temperatures remain consistent with each other. For further analyses of the temperature dependence we decided to keep the full, 5-temperature, line-width data as concerning a larger temperature interval.

The high quality of temperature exponents estimated with the semi-empirically computed

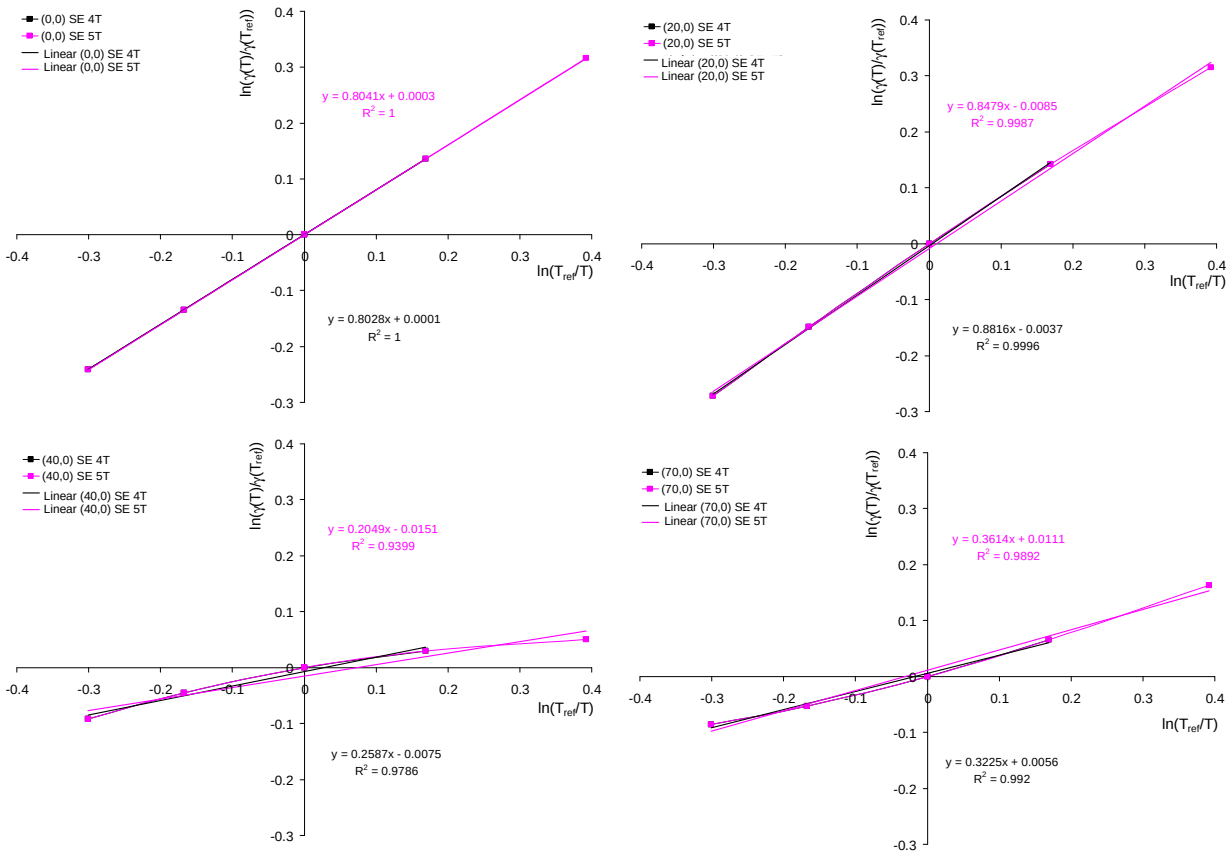

Figure 3: Linear fits of semi-empirical broadening coefficients in log-log coordinates. Linear (for $J \lesssim 20$) or nearly linear (for $J \gtrsim 20$) behavior is observed in all cases. Adding the SE values at 200 K does not change significantly the deduced temperature exponents.

line widths is also confirmed by the broadening coefficients restored for the considered temperatures of 200, 250, 296, 350 and 400 K. Examples are shown on the left-side panels of Fig. 5 for $^{\mathrm{R}}$R transitions with K=0, 10 and 20.

3.3. Extraction of double power law parameters

The non-linear behavior of $\log(\gamma(T)/\gamma(T_{ref}))$ on $\log(T_{ref}/T)$ in large temperature intervals observed for many molecular systems has initiated very recently an advanced study of line width and shift temperature dependence by Gamache and Vispoel [18]. They suggested four-parameter laws for both line widths and shifts which account for a correction term to the usual expression of Eq.(9) (the so-called double power law — DPL):

$$\gamma_{if}(T) = a_1 \left(\frac{T}{T_{ref}}\right)^{n_1} + a_2 \left(\frac{T}{T_{ref}}\right)^{n_2} \tag{10}$$

In our case of CH_3I, as mentioned above, the semi-empirical line widths calculated at various temperatures are very well fitted by the usual equation with temperature exponents.

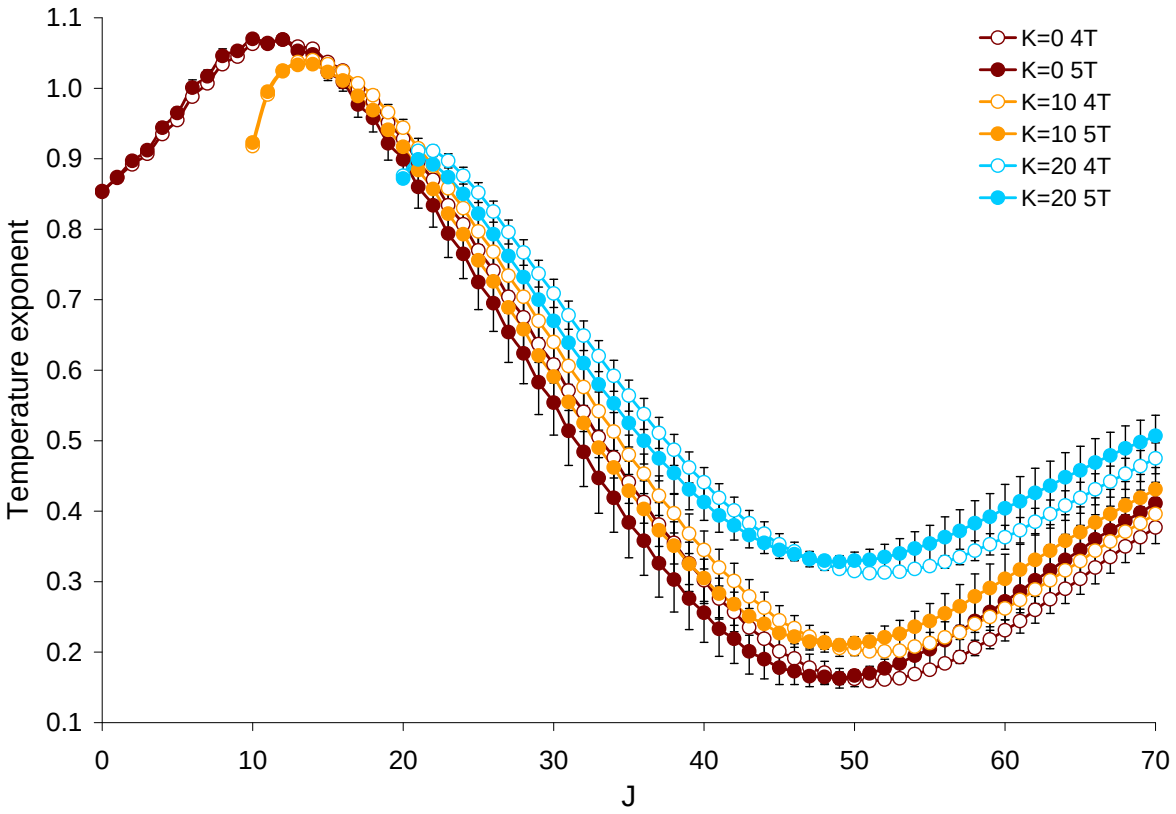

Figure 4: SE temperature exponents extracted for $^{\mathrm{R}}$R transitions with some specific K values using the line-broadening data for 4 (250, 296, 350, 400 K) and 5 (200, 250, 296, 350, 400 K) temperatures. The differences are very small for $J \lesssim 20$ and near $J \approx 47 - 49$; they grow up to ≈ 0.04 for the other J but still remain inside the estimated error bars.

For some transitions, however, a non-linear behavior in the log-log coordinates was stated, so that we attempt to apply the DPL approach to these lines. The non linear fit procedure was realized with a modified Levenberg-Marquardt algorithm and a finite-difference Jacobian [32], which require initial guess values for the fitted parameters and are very sensitive to them. The maximal allowed number of iterations was fixed to 400. Because of strong correlations between two terms, direct fits of Eq.(10) were not feasible, and we slightly re-written it as

$$\gamma(T) = a_1 \tilde{T}^{n_1}(1 + a'_2 \tilde{T}^{n'_2}), \tag{11}$$

with $\tilde{T} = T/T_{ref}$. The initial guesses for a_1 and n_1 were taken as $\gamma(T_{ref})$ and N (temperature exponent) issued from the linear-regression fits; the initial values of a'_2 and n'_2 were put equal to 0 and 1, respectively. With this 4-parameter configuration no converged results were obtained with the allowed maximal number of iterations (again, because of the above-mentioned correlations). We attempt therefore a simpler 3-parameter fit with the expression $\gamma(T) = a_1 \tilde{T}^{n_1}(1 + a''_2)$ to see the importance of the correction term. This fit easily provided

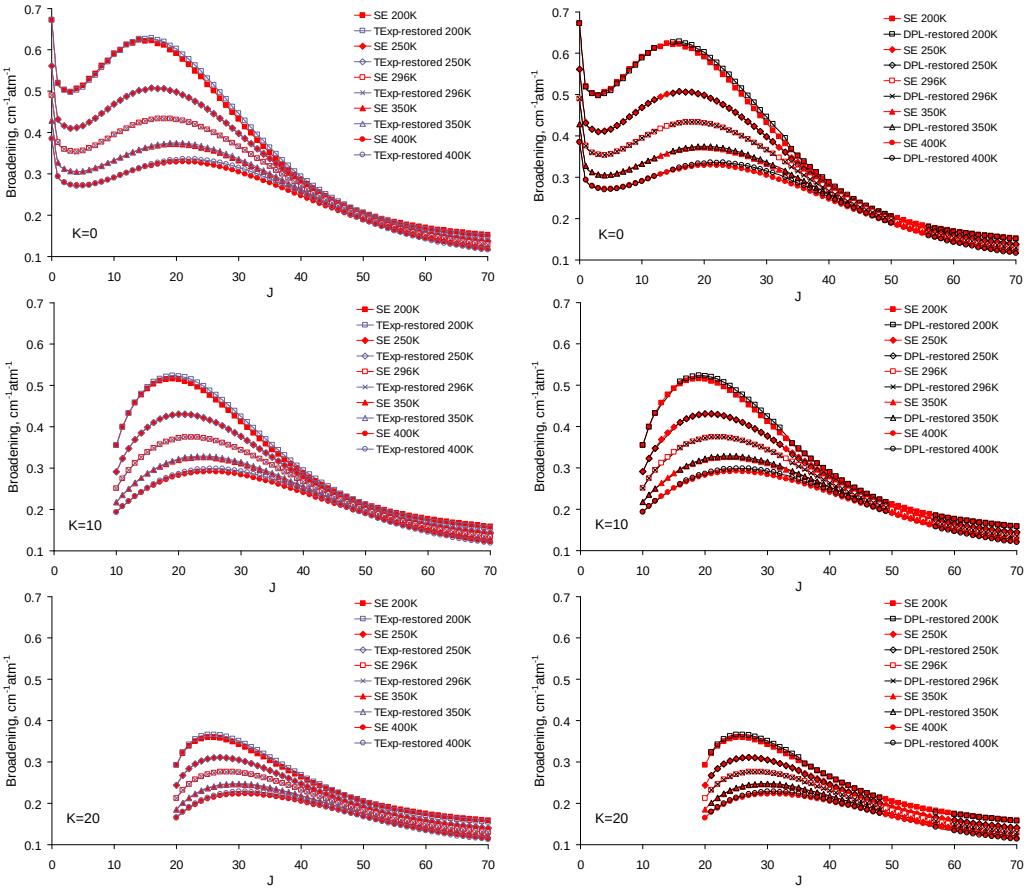

Figure 5: Broadening coefficients restored with the SE temperature exponents (left panels) and with the double power law parameters at 200, 250, 296, 350 and 400 K.

a_1 and n_1 consistent with $\gamma(296)$ and N within below than 1% (meaning that the correction is very small), so that to be able to determine the parameters of the second DPL term, we decided to fix a_1 and n_1 to $\gamma(T_{ref})$ and N. Even with this restriction, a'_2 and n'_2 remained undetermined for some transitions (maximal number of iterations exceeded), so that we considered the single power law of Eq. (9) being sufficient and put $a'_2 = n'_2 = 0$. Moreover, zero values of a'_2, n'_2 were admitted for lines with too small $|a'_2|$ values or too high $|n'_2|$ values (we assumed, respectively, 10^{-4} and 3 as reasonable criteria). An example of deduced parameters is given in Table 2 for $^{\mathrm{R}}$R transitions with $K = 0$ and $K = 20$. It can be seen from this table that the second power term in Eq.(10) introduces very small corrections, and for many lines this simple law with a temperature exponent works very well. This fact is confirmed by the plots in the rhs of Fig. 5: the line widths restored with the double power law are practically identical to those restored with the single power law. Some "holes" appearing on DPL curves indicate the transitions for which the DPL fits were not converged and $a'_2 = n'_2 = 0$ were assumed. Slightly higher quality of restoring the broadening with the DPL parameters is observable on 200 K-curves at high J values ($\gtrsim 55$). The full set of DPL parameters for $0 \leq J \leq 70$, $K \leq 20$ transitions in the 6 sub-branches of the ν_6 band is given in Supplementary material.

Similar tests of line widths restored with the temperature exponents and the DPL parameters were done for the SC results. Fig. 6 (left panel) shows that the approach of temperature exponents reproduces very well the room-temprature data but introduces significant deviations from the input line widths at low and high temperatures. The DPL approach demonstrates some discrepancies for the room-temperature values but gives very good results for the other temperatures. Because of the underestimation of broadening at very small J and their overestimation for the mid-range J-values with respect to the room-temperature measurements, we decided to do not include the temperature dependence characteristics deduced with the semi-classical results in our final results listed in Supplementary material.

4. Conclusion

In this paper we analyzed the temperature dependence of CH_3I self-broadening coefficients estimated theoretically by a semi-calssical and a semi-empirical approaches in the temperature range 200–400 K relevant to atmospheric applications. Temperature dependence characteristics were extracted with the use of the traditional temperature-exponent form and the recently suggested double power law. The SC results were found to lead to non-linear dependencies in log-log coordinates and to be less reliable for extracting the temperature-dependence parameters. The SE line widths demonstrated linear or nearly linear behaviors and resulted in high-quality fits of temperature exponents allowing perfect restoring of line widths used for fitting. The double power law was more complex to implement and the sufficiency of the single power law resulted in non stability of second power term parameters and convergence problems. When applicable, it allowed very slight improvements of the restored line widths at high J values.

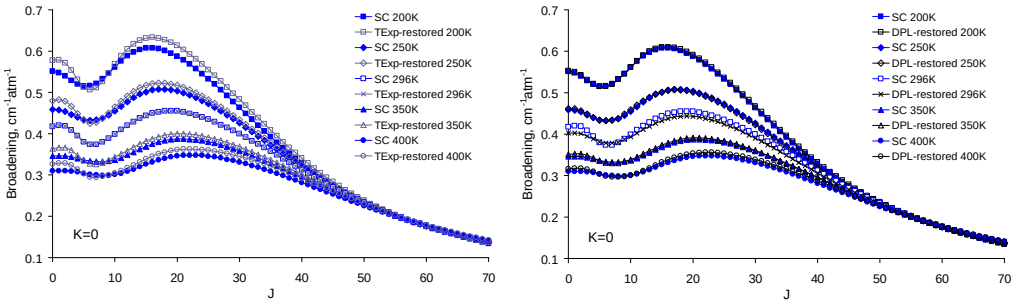

Figure 6: Broadening coefficients restored with the SC temperature exponents (left panels) and with the double power law parameters at 200, 250, 296, 350 and 400 K.

Table 2: Sample of DPL parameters deduced from SE calculations for ^{R}R transitions with K=0 and 20.

	$K=0$					$K=20$			
J	$a_1 \equiv \gamma(T_{ref})$	$n_1 \equiv N$	a'_2, 10^{-3}	n'_2	J	$a_1 \equiv \gamma(T_{ref})$	$n_1 \equiv N$	a'_2, 10^{-3}	n'_2
0	0.4903	0.804	0	0	20	0.2122	0.822	0	0
1	0.3757	0.824	0	0	21	0.2320	0.849	0	0
2	0.3605	0.847	0	0	22	0.2462	0.842	0	0
3	0.3545	0.862	0	0	23	0.2571	0.824	0	0
4	0.3541	0.894	0	0	24	0.2646	0.800	0	0
5	0.3566	0.915	0	0	25	0.2704	0.772	0	0
6	0.3622	0.951	0	0	26	0.2738	0.743	0	0
7	0.3689	0.967	0	0	27	0.2762	0.712	0	0
8	0.3772	0.996	0	0	28	0.2767	0.682	0	0
9	0.3856	1.003	0	0	29	0.2766	0.650	0	0
10	0.3945	1.020	0	0	30	0.2750	0.620	0	0
11	0.4027	1.014	0.4726	2.742	31	0.2731	0.589	0	0
12	0.4106	1.019	0.3355	1.714	32	0.2699	0.560	0	0
13	0.4174	1.003	0	0	33	0.2667	0.530	0	0
14	0.4234	0.998	0	0	34	0.2626	0.503	0	0
15	0.4279	0.973	0	0	35	0.2584	0.475	0	0
16	0.4313	0.959	0	0	36	0.2535	0.450	-7.5359	2.480
17	0.4333	0.927	0	0	37	0.2488	0.425	-7.6024	2.416
18	0.4341	0.908	0	0	38	0.2435	0.404	-7.7178	2.194
19	0.4335	0.872	0	0	39	0.2385	0.381	-8.1526	1.790
20	0.4318	0.849	0	0	40	0.2329	0.363	-7.6366	1.758

In the absence of measurements at not-room temperatures, the deduced temperature-dependence parameters are expected to provide good estimates of line broadening for the studied temperature interval. They may be therefore recommended for spectroscopic databases and atmospheric applications.

Acknowledgements

The authors are grateful for the financial support of LIA SAMIA (Laboratoire International Associé "Spectroscopie d'Absorption de Molécules d'Intérêt Atmosphérique et planétologique: de l'innovation instrumentale à la modélisation globales et aux bases de données") and the Russian Foundation of Fundamental Research (grant №17-52-16022).

Supplementary material

Supplementary material associated with this article can be found at ...

References

[1] Bell N, Hsu L, Jacob DJ, Schultz MG, Blake DR, Butler JH, et al. Methyl iodide: Atmospheric budget and use as a tracer of marine convection in global models. J Geophys Res 2002;107(D17):ACH 8–1–ACH 8–12. https://doi.org/10.1029/2001JD001151.

[2] Fortin C, Fèvre-Nollet V, Cousin F, Lebègue P, Louis F. Box modelling of gas-phase atmospheric iodine chemical reactivity in case of a nuclear accident. Atmos Environ 2019;214:116838. https://doi.org/10.1016/j.atmosenv.2019.116838.

[3] Lim YK, Phang SM, Abdul Rahman N, Sturges WT, Malin G. Halocarbon emissions from marine phytoplankton and climate change. Int J Environ Sci and Tech 2017;14(6):1355–70. https://doi.org/10.1007/s13762-016-1219-5.

[4] Ban-nai T, Muramatsu Y, Amachi S. Rate of iodine volatilization and accumulation by filamentous fungi through laboratory cultures. Chemosphere 2006;65(11):2216 – 22. https://doi.org/10.1016/j.chemosphere.2006.05.047.

[5] Redeker K, Wang NY, Low J, McMillan A, Tyler S, Cicerone R. Emissions of methyl halides and methane from rice paddies. Science 2000;290(5493):966–9. https://doi.org/10.1126/science.290.5493.966.

[6] Rasmussen RA, Khalil MAK, Gunawardena R, Hoyt SD. Atmospheric methyl iodide (CH_3I). J Geophys Res 1982;87(C4):3086–90. https://doi.org/10.1029/JC087iC04p03086.

[7] Gordon I, Rothman L, Hill C, Kochanov R, Tan Y, Bernath P, et al. The HITRAN2016 molecular spectroscopic database. J Quant Spectrosc Radiat Transfer 2017;203:3–69. https://doi.org/10.1016/j.jqsrt.2017.06.038.

[8] Jacquinet-Husson N, Armante R, Scott N, Chédin A, Crépeau L, Boutammine C, et al. The 2015 edition of the GEISA spectroscopic database. J Mol Spectrosc 2016;327:31–72. https://doi.org/10.1016/j.jms.2016.06.007.

[9] Perrin A, Haykal I, KwabiaTchana F, Manceron L, Doizi D, Ducros G. New analysis of the ν_6 and $2\nu_3$ bands of methyl iodide (CH_3I). J Mol Spectrosc 2016;324:28 – 35. https://doi.org/https://doi.org/10.1016/j.jms.2016.04.014.

[10] Kwabia-Tchana F, Attafi Y, Manceron L, Doizi D, Auwera JV, Perrin A. Line intensities for the 6 and $2\nu_3$ bands of methyl iodide ($^{12}CH_3I$). J Quant Spectrosc Radiat Transfer 2019;222-223:130 – 7. https://doi.org/10.1016/j.jqsrt.2018.10.001.

[11] Boughdiri A, Manceron L, Maaroufi N, Rotger M, Aroui H. Measurements of line intensities for some lines of methyl iodide in the ν_5 and $\nu_3 + \nu_6$ bands. J Quant Spectrosc Radiat Transfer 2018;221:147 – 54. https://doi.org/10.1016/j.jqsrt.2018.10.004.

[12] Belli S, Buffa G, Lieto AD, Minguzzi P, Tarrini O, Tonelli M. Hyperfine Level Dependence of the Pressure Broadening of CH_3I Rotational Transitions in the $v_6 = 1$ Vibrational State. J Mol Spectrosc 2000;201(2):314 – 8. https://doi.org/10.1006/jmsp.2000.8106.

[13] Hoffman K, Davies P. Pressure broadening coefficients of ν_5 fundamental band lines of CH_3I at 7μm measured by diode laser absorption spectroscopy. J Mol Spectrosc 2008;252(2):101 – 7. https://doi.org/10.1016/j.jms.2008.07.004.

[14] Raddaoui E, Troitsyna L, Dudaryonok A, Soulard P, Guinet M, Aroui H, et al. Line parameters measurements and modeling for the ν_6 band of CH_3I: A complete line list for atmospheric databases. J Quant Spectrosc Radiat Transfer 2019;232:165 – 79. https://doi.org/10.1016/j.jqsrt.2019.04.036.

[15] Attafi Y, Hassen AB, Aroui H, Tchana FK, Manceron L, Doizi D, et al. Self and N_2 collisional broadening of rovibrational lines in the v_6 band of methyl iodide ($^{12}CH_3I$) at room temperature: The J and K dependence. J Quant Spectrosc Radiat Transfer 2019;231:1 – 8. https://doi.org/10.1016/j.jqsrt.2019.04.017.

[16] Buldyreva J, Guinet M, Eliet S, Hindle F, Mouret G, Bocquet R, et al. Theoretical and experimental studies of CH_3X–Y2 rotational line shapes for atmospheric spectra modelling: application to room-temperature CH_3Cl–O_2. Phys Chem Chem Phys 2011;13:20326–34. https://doi.org/10.1039/C1CP22232E.

[17] Bykov A, Lavrentieva N, Sinitsa L. Semi-empiric approach to the calculation of

H_2O and CO_2 line broadening and shifting. Mol Phys 2004;102(14-15):1653–8. https://doi.org/10.1080/00268970410001725765.
[18] Gamache RR, Vispoel B. On the temperature dependence of half-widths and line shifts for molecular transitions in the microwave and infrared regions. J Quant Spectrosc Radiat Transfer 2018;217:440 – 52. https://doi.org/10.1016/j.jqsrt.2018.05.019.
[19] Ma Q, Tipping RH, Boulet C. Modification of the Robert–Bonamy formalism in calculating Lorentzian half-widths and shifts. J Quant Spectrosc Radiat Transfer 2007;103:588–96.
[20] Bray C, Jacquemart D, Lacome N, Guinet M, Cuisset A, Eliet S. Self-broadening coefficients of methyl chlorid transitions at room temperature J Quant Spectrosc Radiat Transfer 2013; 116:87–103 http://dx.doi.org/10.1016/j.jqsrt.2012.09.013.
[21] Ma Q, Boulet C and Tipping RH. Refinement of the Robert-Bonamy formalism: Considering effects from the line coupling. J Comp Phys 2013;139:034305 http://dx.doi.org/10.1063/1.4813234.
[22] Robert, D, Bonamy, J. Short range force effects in semiclassical molecular line broadening calculations. J Phys Fr 1979;40(10):923–43. https://doi.org/10.1051/jphys:019790040010092300.
[23] Werth S, Horsch M, Hasse H. Surface tension of the two center Lennard-Jones plus point dipole fluid. J Chem Phys 2016;144(5). https://doi.org/10.1063/1.4940966.
[24] Lerot C, Blanquet G, Bouanich JP, Walrand J, Lepère M. Self-broadening coefficients in the ν_2 and ν_5 bands of $^{12}CH_3F$ at 183 and 298 K. J Mol Spectrosc 2005;230(2):153–60. https://doi.org/10.1016/j.jms.2004.11.008.
[25] Gomez L, Jacquemart D, Bouanich JP, Boussetta Z, Aroui H. Theoretical calculations of self-broadening coefficients in the ν_6 band of CH_3Br. J Quant Spectrosc Radiat Transfer 2010;111(9):1252–61. https://doi.org/10.1016/j.jqsrt.2010.01.009.
[26] Dudaryonok A, Lavrentieva N, Buldyreva J. CH_3Cl self-broadening coefficients and their temperature dependence. J Quant Spectrosc Radiat Transfer 2013;130:321 – 6. https://doi.org/10.1016/j.jqsrt.2013.07.013.
[27] Dudaryonok A, Lavrentieva N, Buldyreva J. CH_3CN self-broadening coefficients and their temperature dependences for the Earth and Titan atmospheres. Icarus 2015;250:76 – 82. https://doi.org/10.1016/j.icarus.2014.11.020.
[28] Carocci S, Di Lieto A, Minguzzi P, Tonelli M. Measurement of the electric dipole moment of methyl lodide. J Mol Spectrosc 1990;144(2):429–42. https://doi.org/10.1016/0022-2852(90)90228-I.
[29] Wensink W, Noorman C, Dijkerman H. Self-broadening and self-shifting of J=0 to 1 and J=1 to 2 rotational transitions of CH_3Br and CH_3I. J Phys B 1980;13(20):4007–20. https://doi.org/10.1088/0022-3700/13/20/014.
[30] Tsao C, Curnutte B. Line-widths of pressure-broadened spectral lines. J Quant Spectrosc Radiat Transfer 1962;2(1):41 – 91. https://doi.org/10.1016/0022-4073(62)90013-4.
[31] Dudaryonok A, Lavrentieva N, Buldyreva J. CH3Cl self-broadening coefficients and their temperature dependences. J Quant Spectrosc Radiat Transfer;130:321–6 http://dx.doi.org/10.1016/j.jqsrt.2013.07.013.
[32] Moré JJ. The Levenberg-Marquardt algorithm: Implementation and theory. Numer Anal 1978;630. https://doi.org/10.1007/BFb0067700.